High-fat diet and FGF21 cooperatively promote aerobic thermogenesis in mtDNA mutator mice

Christopher E. Wall[a,b], Jamie Whyte[a], Jae M. Suh[a], Weiwei Fan[a], Brett Collins[a], Christopher Liddle[c], Ruth T. Yu[a], Annette R. Atkins[a], Jane C. Naviaux[d], Kefeng Li[d], Andrew Taylor Bright[d], William A. Alaynick[d], Michael Downes[a], Robert K. Naviaux[d,e], and Ronald M. Evans[a,f,1]

[a]Gene Expression Laboratory, Salk Institute, La Jolla, CA 92037; [b]Biomedical Sciences Graduate Program, University of California at San Diego, La Jolla, CA 92093; [c]The Storr Liver Unit, Westmead Millennium Institute and University of Sydney, Westmead Hospital, Westmead, NSW 2145, Australia; [d]The Mitochondrial and Metabolic Disease Center, Departments of Medicine, Pediatrics, Pathology, and Neurosciences, University of California at San Diego School of Medicine, San Diego, CA 92103; [e]Veterans Affairs Center for Excellence in Stress and Mental Health, La Jolla, CA 92161; and [f]Howard Hughes Medical Institute, Salk Institute, La Jolla, CA 92037

Contributed by Ronald M. Evans, May 29, 2015 (sent for review April 22, 2015; reviewed by Johan Auwerx, David D. Moore, and Junichiro Sonoda)

Mitochondria are highly adaptable organelles that can facilitate communication between tissues to meet the energetic demands of the organism. However, the mechanisms by which mitochondria can nonautonomously relay stress signals remain poorly understood. Here we report that mitochondrial mutations in the young, preprogeroid polymerase gamma mutator (POLG) mouse produce a metabolic state of starvation. As a result, these mice exhibit signs of metabolic imbalance including thermogenic defects in brown adipose tissue (BAT). An unexpected benefit of this adaptive response is the complete resistance to diet-induced obesity when POLG mice are placed on a high-fat diet (HFD). Paradoxically, HFD further increases oxygen consumption in part by inducing thermogenesis and mitochondrial biogenesis in BAT along with enhanced expression of fibroblast growth factor 21 (FGF21). Collectively, these findings identify a mechanistic link between FGF21, a long-known marker of mitochondrial disease, and systemic metabolic adaptation in response to mitochondrial stress.

mitochondria | brown fat | thermogenesis | FGF21 | polymerase gamma

Certain types of mitochondrial stress such as exercise, mitochondrial DNA mutations, or drugs that destabilize the electron transport chain can stimulate a compensatory response that induces mitochondrial biogenesis and improves function (1). However, progressive damage to the mitochondria can eventually overcome any protective effects, leading to dysfunction (2). Recent studies have demonstrated that benefits caused by mild mitochondrial stress can be transmitted nonautonomously to tissues unaffected by the initial insult, and have linked this phenomenon to longevity (3, 4). These studies have provided mechanistic insight into how localized energetic stress on tissues such as skeletal muscle and heart triggered by endurance exercise can have a profound systemic impacts on glucose homeostasis and metabolic plasticity (5). Similarly, studying the molecular basis for the metabolic phenotype of mouse models of mitochondrial disease has the potential to more fully illuminate the pathways targetable by mitochondrial-based therapies for metabolic disorders.

One such model is the polymerase gamma mutator (POLG) mouse, a progeroid mouse model in which extensive studies have mechanistically coupled mitochondrial DNA mutations and aging (6). These mice express a proofreading-deficient version of the nuclear-encoded mitochondrial DNA polymerase gamma and, consequently, accumulate point mutations and deletions in their mitochondrial genome (7). These mice display a premature aging phenotype that substantially manifests around 9 mo of age with symptoms such as weight loss, s.c. lipodystrophy, alopecia, infertility, and anemia, ultimately resulting in death around 12 mo (6). Despite being conceptualized as a simple model of progeria, an increasing number of recent studies have suggested that the POLG phenotype is more complicated. For example, an endurance exercise intervention was reportedly able to impede the manifestation of progeria (8). Despite the apparent accumulation of mitochondrial defects, POLG mice lack signs of increased reactive oxygen species (ROS), with only recent evidence of oxidative damage in skeletal muscle (9, 10). Moreover, most mitochondrial DNA mutations occur during embryogenesis and are evident by 2 mo of age, although young POLG mice do not exhibit any apparent signs of respiratory chain dysfunction or progeria (6, 11).

Whereas the mitochondrial dysfunction present in the aging POLG mouse has been extensively characterized, the younger, preprogeroid POLG mouse remains largely unexplored. Given the long gap between the initial mitochondrial mutations and the development of any apparent signs of mitochondrial dysfunction, we hypothesized that young POLG mice may elicit compensatory mechanisms to maintain mitochondrial function before succumbing to accumulating damage from dysfunctional mitochondria as they age (6). We find that young POLG mice mimic a metabolic state of starvation, which confers resistance to diet-induced obesity and the pathologies that accompany it. Interestingly, this response

Significance

Fibroblast growth factor 21 (FGF21), a hormone that mediates an adaptive response to starvation, is also a long-standing marker of mitochondrial disease. In this article, we describe the metabolic benefits induced by mild mitochondrial stress via FGF21 induction in polymerase gamma mtDNA mutator (POLG) mice, a model of mitochondrial disease and premature aging. When challenged with a high-fat diet (HFD), these mice resist diet-induced obesity and its underlying associated disease states. In addition, nutrients from a HFD appear to reverse metabolic imbalance in these mice. HFD also robustly increases fat metabolism and improves mitochondrial function in brown fat, which mediates adaptive thermogenesis. Hence, we highlight a metabolically favorable synergy between mitochondrial stress and HFD facilitated by FGF21 in this mouse.

Author contributions: C.E.W., J.W., J.M.S., W.F., B.C., R.T.Y., A.R.A., M.D., and R.M.E. designed research; C.E.W., J.W., W.F., B.C., and A.T.B. performed research; J.C.N., K.L., A.T.B., and R.K.N. contributed new reagents/analytic tools; C.E.W., W.F., C.L., R.T.Y., A.R.A., J.C.N., K.L., A.T.B., W.A.A., M.D., and R.K.N. analyzed data; and C.E.W., R.T.Y., A.R.A., M.D., and R.M.E. wrote the paper.

Reviewers: J.A., Ecole Polytechnique Fédérale de Lausanne; D.D.M., Baylor College of Medicine; and J.S., Genentech.

The authors declare no conflict of interest.

Freely available online through the PNAS open access option.

Data deposition: The RNA-sequence reads reported in this paper have been deposited at the National Center for Biotechnology Information (NCBI) Sequence Read Archive (accession no. SRP057650).

[1]To whom correspondence should be addressed. Email: evans@salk.edu.

This article contains supporting information online at www.pnas.org/lookup/suppl/doi:10.1073/pnas.1509930112/-/DCSupplemental.

can be attenuated through a paradoxical induction of catabolism by a calorie-rich high-fat diet (HFD). Moreover, HFD rescues thermogenic defects in these mice by inducing mitochondrial biogenesis in brown adipose tissue (BAT). Furthermore, we demonstrate that this protective response to HFD in BAT requires the endocrine hormone fibroblast growth factor 21 (FGF21). These results link FGF21, a long-known marker of mitochondrial dysfunction, to how mitochondrial signaling can affect metabolic plasticity, and highlight the potential therapeutic value of using drugs that stress mitochondria to treat metabolic diseases such as obesity.

Results

Mitochondrial Mutations in Young POLG Mice Confer Resistance to Diet-Induced Obesity. To evaluate how young POLG mice adapt to metabolic stress, we challenged 2.5-mo-old cohorts of these mice (along with relevant controls) with a HFD (60% kcal from fat) for 2 mo. Surprisingly, POLG mice were completely resistant to weight gain throughout the entirety of this dietary regimen (Fig. 1*A*). Magnetic resonance imaging of body fat composition revealed that POLG mice on a chow diet have reduced body fat (~50%) compared with HFD-fed WT controls, making their adiposity equivalent to WT mice on chow (Fig. 1*B*). To explain this apparent resistance to diet-induced obesity (DIO), we first used the Oxymax/Comprehensive Lab Animal Monitoring System (CLAMS) cage system to measure metabolic rate in these mice by way of oxygen consumption (VO2) and respiratory exchange ratios (RER; VCO2/VO2). Unexpectedly, we observed that HFD actually increases VO2 by 1.8-fold in POLG mice during both light and dark cycles (Fig. 1*C* and Fig. S1*A*). In addition, both chow and HFD-fed POLG mice have a lower RER during the light cycle in comparison with chow-fed WT mice (0.82 vs. 0.87), signifying a preference for fat as a metabolic substrate (Fig. 1*D* and Fig. S1*B*). We next examined food consumption and activity over the course of the 2-mo high-fat dietary challenge. POLG mice fed either chow or HFD both consume a similar amount of calories per day (10-11kcal/d on chow and 14–15kcal/d on HFD) and have approximately similar patterns of activity during both the light and dark cycles in comparison with WT controls (Fig. S1 *C* and *D*). We next asked whether HFD-fed POLG mice maintain underlying metabolic health in addition to remaining lean by measuring fasting levels of glucose and insulin. First, chow-fed POLG mice have 1.2-fold lower glucose and 1.4-fold lower insulin levels than WT controls (Fig. 1 *E* and *F*). Similarly, on HFD, POLG mice also have reduced glucose (−1.3 fold) and insulin (−1.9 fold) levels in comparison with WT mice fed HFD (Fig. 1 *E* and *F*). Next, we measured fasting blood levels of several endocrine hormones that regulate metabolism. On a chow diet, POLG mice have a 1.8-fold increase in the hunger-promoting hormone ghrelin, with a 5.6-fold decrease in the hunger-suppressing hormone leptin (Fig. S2 *A* and *B*). However, POLG mice on a HFD have comparatively similar levels of both hormones to WT mice fed chow (Fig. S2 *A* and *B*). Moreover, POLG mice fed HFD have markedly reduced levels of resistin and PAI-1 in comparison with WT controls, which are hormone markers of obesity and metabolic syndrome (Fig. S2 *C* and *D*). Furthermore, POLG mice fed chow have dramatically increased (4.7-fold) levels of fibroblast growth factor 21 (FGF21), an endocrine hormone known to mediate an adaptive response to starvation (Fig. 1*G*) (12). Interestingly, HFD appears to synergistically increase FGF21 levels in POLG mice to roughly ninefold higher in comparison with WT mice fed chow or HFD (Fig. 1*G*). Collectively, we observed that preprogeroid POLG mice on a chow diet display several hallmarks of a metabolic starvation-like state. This response can be alleviated by placing these mice on a HFD, which induces a striking increase in aerobic respiration and confers resistance to diet-induced obesity.

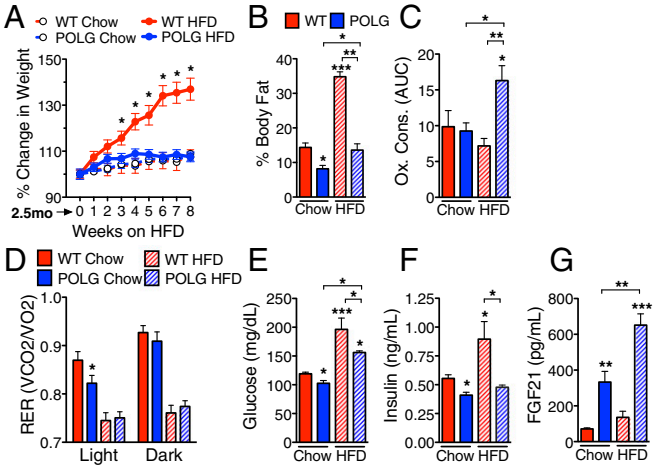

Fig. 1. POLG mice resist diet-induced obesity through mimicking a metabolic state of starvation. (*A*) Changes in whole body weight in 2.5-mo-old WT and POLG mice fed either Chow or HFD for 8 wk. (*B*) Body fat composition as determined by MRI. (*C*) CLAMS cabinet measurement of the oxygen consumption rate at 22 °C (VO2, $mL{\cdot}kg^{-1}{\cdot}h^{-1}$) by area under the curve (AUC) after 8 wk of HFD, over the course of a 24-h Zeitgeber day (also see Fig. S1*A*). (*D*) Mean respiratory exchange ratios (CO_2 emission/O_2 consumption) during the light and dark cycles. Quantification of fasting blood glucose (*E*), insulin (*F*), and FGF21 (*G*) levels after 8 wk on chow or HFD. Data are represented as mean ± SEM, $n = 9$–10 per group (*A*, *B*, *D*, and *E*), 4 per group (*C*). $^*P \leq 0.05$, $^{**}P \leq 0.005$, $^{***}P \leq 0.0005$ versus WT Chow unless otherwise noted.

HFD Reverses Metabolic Imbalance in Young POLG Mice. How might additional nutrients supplied by a HFD impact the apparent metabolic state of starvation in chow-fed POLG mice? To investigate this question, we first examined changes in global patterns of gene expression in liver and white fat from HFD-fed POLG mice and controls using RNA-Seq. We first used gene ontology analyses to identify biological processes that were highly regulated by mitochondrial mutations and/or HFD feeding, and generated heat maps displaying expression patterns of genes involved in these processes (Fig. 2 *A* and *B*). For each gene, the expression value is displayed as the log-transformed difference from the mean value of the four cohorts of mice. In both liver and white fat, we found that genes that mediate metabolic processes, such as glucose or fatty acid metabolism and energy production, have inverse patterns of expression in POLG Chow compared with WT HFD, and similar patterns of expression when comparing WT Chow to POLG HFD (Fig. 2 *A* and *B*). This finding suggests that starvation and nutrient excess induce divergent adaptive changes in gene expression in liver and white fat, both of which are diminished in POLG mice fed a HFD. To explore the functional metabolic consequences of these divergent transcriptional responses to mitochondrial mutations and HFD, we next conducted metabolomic analysis on plasma taken from the four described cohorts of mice using liquid chromatography-tandem mass spectrometry (LC-MS/MS). Five hundred eighty-two metabolites from 60 biochemical pathways were measured, and principle component based variable importance in projection (VIP) scores were assigned to the top metabolites that were distinguishable between diet and genotype. Partial least squares discriminate analysis (PLSDA) was used to correlate the metabolome from each of the four cohorts of mice based on two components consisting of metabolites selected for VIP scores >1.5 (13). Based on this analysis, the comprehensive WT Chow metabolomic profile is centralized between that of POLG Chow and WT HFD, with POLG HFD appearing to trend between the opposing extremes of POLG Chow and WT HFD as well (Fig. 2*C*). In addition, correction of disease states associated with obesity were also evident in HFD-fed POLG

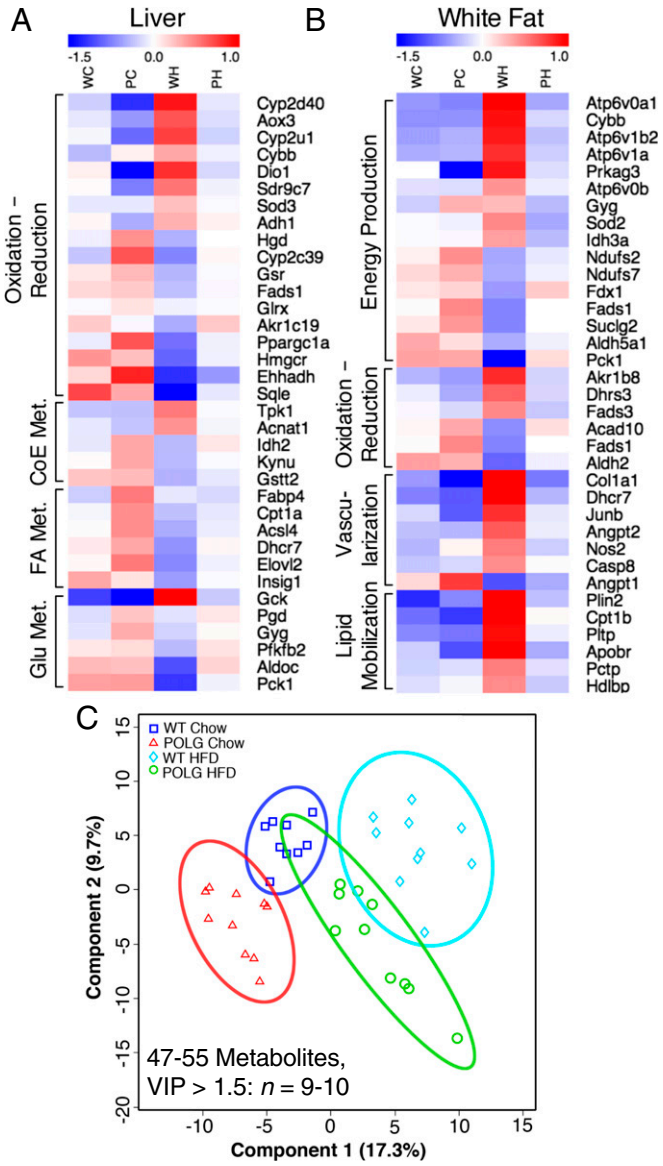

Fig. 2. HFD reprograms gene expression in POLG mice and restores metabolic imbalance. (*A* and *B*) Rank-ordered expression of key genes from differentially regulated biological processes in liver and white fat for 4.5 mo WT and POLG mice fed either Chow or HFD after 8 wk (PC, POLG Chow; PH, POLG HFD; WC, WT Chow; WH, WT HFD). The heat maps represent the $\log_2$ of the fold-change of each group compared with the mean fragments per kilobase of exon per million fragments mapped for each gene as determined through RNA-Seq. (*C*) Multivariate PLSDA of component groups of plasma metabolites significantly different between WT Chow, POLG Chow, WT HFD, and POLG HFD mice. $n = 3$ per group (*A* and *B*), 9–10 per group (*C*).

mice. For example, we observed that livers from POLG mice are completely resistant to HFD-induced steatosis (Fig. S3*A*). Similarly, a hematoxylyn and eosin (H&E) stain of white adipose tissue (WAT) revealed that adipocyte size mirrors body fat composition in these mice (Fig. S3 *B* and *C*). POLG mice on a HFD also have significantly reduced expression of obesogenic gene markers of macrophage infiltration and inflammation in their white fat in comparison with WT-fed HFD (Fig. S3*D*). Taken together, these data propose that the opposing metabolic adaptations to mitochondrial mutations and elevated nutrients are balanced in preprogeroid POLG mice fed a HFD to more closely resemble a normal lean mouse.

HFD Rescues Thermogenic Defects and Causes Mitochondrial Biogenesis in BAT. What tissue might be responsible for the increase in oxygen consumption and lipid metabolism observed in POLG mice-fed HFD? BAT, which mediates adaptive nonshivering thermogenesis, seemed to be a likely candidate considering that it is dense with mitochondria and can undergo a substantial increase in energy expenditure upon stimulation (14). In addition, recent studies have established the sensitivity of BAT to stimulation through FGF21, which we also observed to be highly elevated in POLG mice fed a HFD (15, 16). Because BAT functionality in POLG mice has not previously been described, we first explored the impact of diet by using a thermal infrared camera to quantify radiated heat from the scapular region. Surprisingly, we found that POLG mice on chow produce much less heat than WT, with a 2 °C lower mean surface temperature in this area (Fig. 3 *A* and *B*). This apparent thermogenic defect can be partially rescued by placing these mice on HFD, which elevates the surface temperature by 1 °C (Fig. 3 *A* and *B*). Histologically, BAT from WT and POLG mice-fed chow appears to have a comparable fat content, whereas BAT from WT mice on a HFD contains 1.5-fold more stored fat (Fig. 3*C*). However, POLG mice fed a HFD have half the amount of fat in their BAT compared with WT and POLG chow, with the larger lipid droplets appearing to have all but disappeared (Fig. 3*C* and Fig. S4*D*). Moreover, HFD appears to increase the eosinophilic content of POLG BAT, consistent with an induction of fat browning and thermogenesis (17) (Fig. 3*C*). Trichrome staining failed to show evidence of fibrosis, whereas a Verhoeff stain revealed a dense elastin network induced in POLG BAT by HFD (Fig. S4 *A* and *B*).

To investigate whether the increase in radiated heat and depletion of lipids from BAT in POLG mice on a HFD might be attributable to a restoration of thermogenic metabolism, we examined protein levels of UCP1, which mediates uncoupling of protons across the electron transport chain in mitochondria to generate heat. In POLG mice, HFD appears to dramatically induce UCP1 protein expression in BAT as evidenced by both Western blot and immunohistochemistry (Fig. 3 *D* and *E*). Differences in UCP1 protein expression levels between WT and POLG mice fed chow or HFD are also similar to the observed differences in surface temperature (Fig. S4*C*). In addition, genes responsible for mediating thermogenesis are down-regulated in BAT from POLG mice fed chow in comparison with WT, and rescued to (or even up-regulated beyond) WT levels when POLG mice are placed on HFD (Fig. 3*F*). Inflammation in BAT has also been linked to thermogenesis through an induction of UCP1 (18), and several inflammatory gene markers (including *Cd68, Tlr1, Tnfaip8l2,* and *Mmp12*) are induced by HFD in BAT from POLG mice (Fig. S4*E*).

The above results prompted us to explore whether the thermogenic adaptation to HFD exhibited by POLG mice includes induction of mitochondrial biogenesis in BAT. To answer this question, we examined the mitochondrial structure and content in BAT from WT and POLG mice on chow or HFD directly. Initially, we used electron microscopy (EM) to image the mitochondria in BAT from each of the four cohorts. Normal BAT mitochondria are ∼1 μm across and appear to be localized between the larger lipid droplets, as shown by WT chow and WT HFD (Fig. 4*A*). In contrast, BAT from POLG mice on chow contained enlarged (5–6 μm diameter) mitochondria, a hallmark of mitochondrial dysfunction (19) (Fig. 4*A*). Interestingly, large mitochondria are no longer evident in POLG BAT when the mice are placed on HFD (Fig. 4*A*). Quantification of the average number of cristae per square micrometer in these mitochondria revealed that HFD is able to reverse the defective 3.1-fold lower ratio in POLG chow back to that of WT controls (Fig. 4*B*). We next quantified the amount of mitochondria in BAT directly through quantitative PCR (qPCR). Strikingly, HFD increases the mitochondrial DNA content (normalized to nuclear DNA content) of POLG BAT

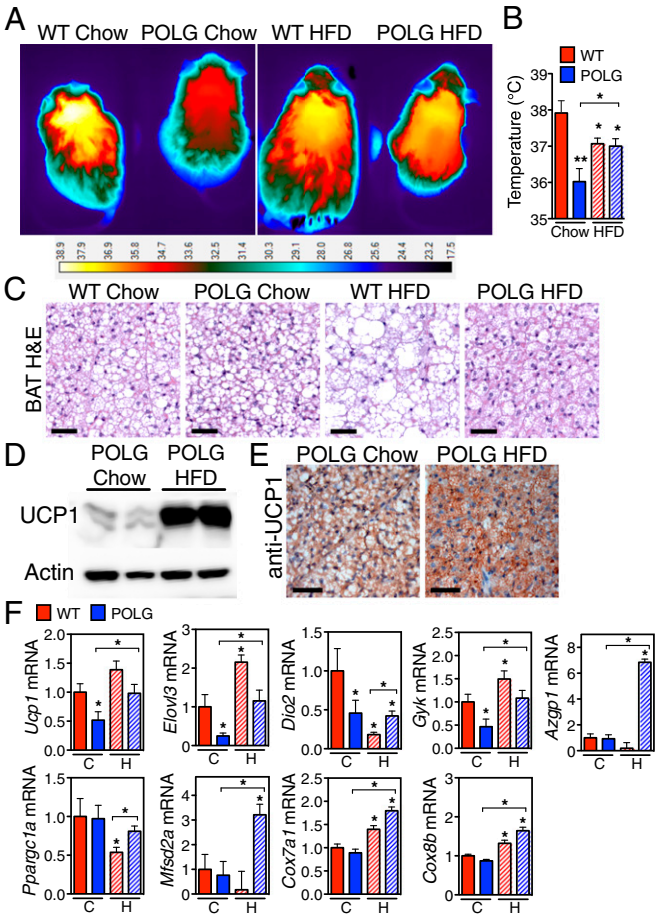

Fig. 3. Thermogenic defects in POLG brown adipose tissue are rescued by HFD. (*A*) Surface temperature of radiated heat visualized by infrared camera in 4.5 mo WT and POLG mice fed either Chow or HFD after 8 wk. (*B*) Quantification of the mean surface temperature in the scapular region above the BAT. (*C*) H&E stained sections from BAT. (*D*) UCP1 Western blot in BAT protein lysates from chow and HFD-fed POLG mice (two mice per group). Actin is used as a loading control (also see Fig. S4*C*). (*E*) UCP1 immunohistochemical staining in sections from chow and HFD-fed POLG mice. (*F*) Quantification of thermogenic gene expression (*Azgp1*, α-2-glycoprotein 1, zinc-binding; *Cox7a1*, cytochrome *c* oxidase polypeptide 7a1; *Cox8b*, cytochrome *c* oxidase polypeptide 8b;*Dio2*, Deiodinase 2; *Elovl3*, fatty acid elongase 3; *Gyk*, glycerokinase; *Mfsd2a*, Major facilitator superfamily domain-containing protein 2; *Ppargc1a*, PPAR γ coactivator 1 α; *Ucp1*, uncoupling protein 1) in BAT via qPCR. C, Chow; H, HFD. Data are represented as mean ± SEM $n = 6$ per group (*B* and *C*), 10 per group (*F*). $^{*}P \leq 0.05$, $^{**}P \leq 0.005$, $^{***}P \leq 0.0005$ versus WT Chow unless otherwise noted. (Scale bars: 25 μm.)

by 1.5-fold over WT controls, signifying a substantial increase in mitochondrial biogenesis (Fig. 4*C*). Similarly, we examined protein expression of the individual mitochondrial electron transport chain (ETC) subunits by Western blot (Complex I–V) and found that BAT from POLG mice on HFD contains significantly more Complex I, II, and III than each of the other groups (Fig. 4*D*). Expression of mitochondrial-encoded genes that compose complexes I, IV, and V of the ETC are also highly induced by HFD in POLG BAT (Fig. 4*E*). Jointly, these data demonstrate that HFD rescues thermogenic defects in POLG BAT through stimulating fat metabolism, activating a thermogenic gene expression program, and inducing mitochondrial biogenesis.

HFD-Induced Mitochondrial Biogenesis in Young POLG BAT Requires FGF21 Expression. Young POLG mice and mice with increased FGF21 activity exhibit several starvation-like traits, including decreased adiposity and BAT thermogenesis (20, 21). Interestingly, although FGF21 is also a well-established marker of mitochondrial disease and dysfunction (22, 23), its precise role in mediating mitochondrial stress and metabolic adaptation has yet to be elucidated. To address this problem, we injected adenoviruses containing either a scrambled (shScram) or short-hairpin RNA targeting FGF21 (shFGF21) into 4-mo-old WT and POLG mice after 6 wk of HFD feeding, generating four experimental cohorts. Adenoviral infection and hepatic shRNA expression was confirmed by qPCR for the eGFP tag on both constructs, and FGF21 knockdown efficiency was validated via ELISA upon completion of the study (Fig. S5 *A* and *B*). One week after injecting the virus, we observed a significant increase in body weight of POLG mice-fed HFD expressing shFGF21 over POLG HFD-expressing shScram (Fig. 5*A*). We also observed significantly reduced blood lactate, a marker of increased glycolysis and mitochondrial dysfunction, in POLG HFD mice with reduced FGF21 compared with shScram (Fig. 5*B*). We next asked whether knocking down FGF21 would be sufficient to ablate any of the adaptive changes in thermogenic gene expression and mitochondrial function in BAT from POLG mice fed a HFD. Indeed, we observed an increase in lipid droplet size and fat content in HFD-fed POLG BAT as measured histologically (Fig. 5 *C* and *D*). In addition, FGF21 knockdown decreased mitochondrial biogenesis in HFD-fed POLG BAT 1 wk after injecting the adenovirus (Fig. 5*E*). We next asked whether FGF21 knockdown could prevent the HFD-induced up-regulation of genes that mediate BAT thermogenesis in POLG mice. Surprisingly, we found that FGF21 loss blunted the induction of thermogenic genes (Fig. 5*F*), mitochondrial-encoded ETC subunits (Fig. 5*G*), and inflammatory marker genes by HFD (Fig. S5*C*) in POLG BAT. These data suggest that hepatic FGF21 directly contributes the adaptive increase in mitochondrial biogenesis and function in POLG BAT caused by a HFD.

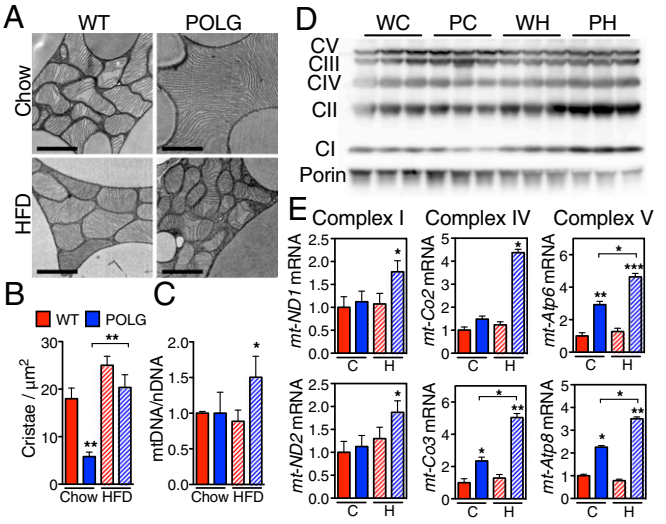

Fig. 4. HFD causes a robust increase in POLG brown adipose tissue mitochondrial biogenesis. Electron microscopy showing mitochondria in BAT from 4.5 mo WT and POLG mice fed either Chow or HFD after 8 wk (*A*), and quantification of the number of cristae per mitochondrial area (square micrometers) (*B*). (Scale bar: 1 μm.) (*C*) Quantification of BAT mtDNA normalized to total genomic DNA by qPCR. (*D*) Immunoblot of proteins from the five ETC complexes (CI, NDUFB8; CII, SDHB; CIII, UQCRC2; CIV, MTCO1; CV, ATP5A) in protein lysates from BAT (three mice per group). Porin is used as a loading control. (*E*) Quantification of mitochondrial gene expression (*ND1/2*, Complex I; *Co2/3*, Complex IV; *Atp6/8*, Complex V) in BAT via qPCR. C, Chow; H, HFD. Data are represented as mean ± SEM, $n = 3$ per group (*A* and *B*), 6 per group (*C*–*E*). $^{*}P \leq 0.05$, $^{**}P \leq 0.005$, $^{***}P \leq 0.0005$ versus WT Chow unless otherwise noted.

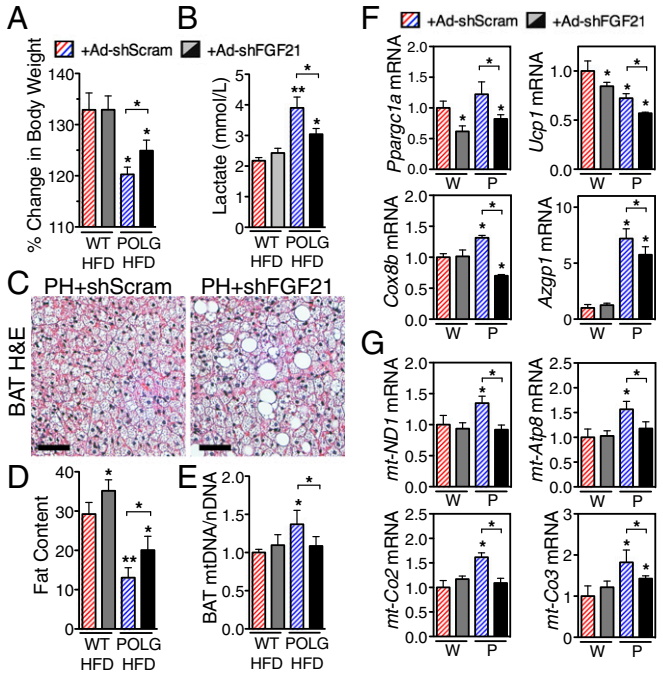

Fig. 5. Hepatic FGF21 knockdown blunts the adaptive thermogenic response to HFD in POLG brown adipose tissue. (*A*) Changes in whole body weight in 4-mo-old WT and POLG mice after 6 wk of HFD feeding, then injected with an adenovirus containing either a scrambled (Ad-shScram) or FGF21-targeted (Ad-shFGF21) shRNA for 1 wk. (*B*) Levels of fasting serum lactate. (*C*) H&E-stained sections from POLG HFD (PH) BAT. (Scale bar: 50 μm.) (*D*) Quantification of total fat content from BAT. (*E*) Quantification of BAT mtDNA normalized to total genomic DNA by qPCR. (*F*) Quantification of thermogenic gene expression (*Azgp1*, α-2-glycoprotein 1, zinc-binding; *Ppargc1a*, PPAR gamma co-activator 1 α; *Ucp1*, uncoupling protein 1) in BAT by qPCR. P, POLG fed HFD; W, WT fed HF. (*G*) Quantification of mitochondrial ETC-subunit gene expression (*mt-Atp8*, Complex V; *mt-Co2/3*: Complex IV; *mt-ND1*, Complex I) in BAT by qPCR. Data are represented as mean ± SEM, $n = 10$ per group. $^{*}P \leq 0.05$, $^{**}P \leq 0.005$, $^{***}P \leq 0.0005$ versus WT HFD + Ad-shScram unless otherwise noted.

Discussion

Mitochondrial function is undoubtedly intertwined with metabolic fitness, but our understanding of the precise mechanism by which mitochondria can communicate to peripheral tissues to regulate metabolism on a systemic scale still remains largely convoluted. In this study, we used a mouse model of mitochondrial dysfunction and progeria, the POLG mouse, to study the mechanisms through which stressed mitochondria can adapt and regulate whole-body metabolism. One might expect these mice to be metabolically maladaptive and respond poorly to energetic stress, but we have surprisingly found that young POLG mice actually exhibit paradoxical improvements in mitochondrial function and metabolic plasticity before they eventually develop signs of progeria. When challenged with a HFD, these mice exhibit common characteristics seen during fasting and starvation in normal mice, becoming resistant to diet-induced obesity, showing improvements in glucose homeostasis, and displaying a metabolic profile phenotypically similar to that of WT mice fed a chow diet. In addition, HFD-fed POLG mice surprisingly increase in their systemic metabolic rate in conjunction with an induction of thermogenesis and mitochondrial biogenesis in BAT.

This metabolic phenotype exhibited by young POLG mice appears to resemble that of mouse models that overexpress FGF21, which mediates the benefits of caloric restriction and is a known marker of mitochondrial stress (12, 24). After observing dramatically increased levels of FGF21 in POLG mice in conjunction with our metabolic findings, we hypothesized that FGF21 might play a role in mediating the POLG resistance to diet-induced obesity. In support of this idea, we found that blunting the induction of FGF21 in POLG mice fed a HFD could suppress at least the induction of mitochondrial biogenesis and genes that mediate thermogenesis in BAT. Given, however, that FGF21-overexpressing mice are widely recognized as a prolongevity model, we believe that our work in POLG mice complicates the concept of a simple antiaging function for FGF21. This idea is also supported by recent compounding evidence demonstrating that FGF21 is also highly induced in many metabolically maladaptive states (25). Instead, we propose that FGF21 functions as a critical transmitter of metabolic demands from stressed mitochondria to other tissues in the body.

Given the difficulties in advancing FGF21 and its analogs in clinical trials (26), how might the FGF21-mediated peripheral beneficial metabolic impacts in POLG mice be exploited therapeutically? Attempts to inject supraphysiological amounts of FGF21 or similar compounds into circulation have been troubled by considerable logistical issues and adverse effects, such as infertility and bone degeneration (27). However, induction of FGF21 by pharmaceuticals that stress the mitochondria might be able to circumvent high dose-related adverse events. One potential example of this idea is metformin, the most widely prescribed antidiabetic drug on the market today, which is believed to function as a mitochondrial inhibitor and has recently been shown to induce FGF21 both in vivo and in vitro (28, 29). Accordingly, we conjecture that similar compounds that cause mitochondrial stress could be used therapeutically in obese individuals with high dietary fat intake to increase lipid metabolism through FGF21 and the BAT. However, we also speculate that patients suffering from mitochondrial diseases could potentially ameliorate some of their metabolic symptoms by increasing the fat content of their diet, thereby supplying additional nutrients to swing their metabolism away from a FGF21-induced starvation-like state.

Despite the known benefits of mild mitochondrial stress, POLG mice still develop a progeroid phenotype and ultimately die prematurely. One recent study has proposed the use of HFD to rescue another model of progeria, Cockayne Syndrome, highlighting a dysregulated PARP1/Sirt1-dependent pathway that drives the premature aging phenotype (30). An important distinction between this study and the one described in this manuscript is that the benefits induced by HFD for Cockayne Syndrome appear to be independent of thermogenesis or increased metabolism of the diet. Therefore, we propose that lipids from a HFD are able to function as a preferential substrate for dysfunctional mitochondria in young POLG mice. FGF21, produced by the liver in response to mitochondrial stress, is able to signal to oxidative peripheral tissues such as BAT to prime their metabolic machinery to be able to process lipids. In support of this idea, we would reason that the POLG mouse progresses along a gradient of increasing stress from mitochondrial mutations as it ages, which at a certain stage will tip the scales between the starvation-like benefits mediated by FGF21 at a young age to unavoidable metabolic dysfunction. Indeed, the pathological metabolic state evident in old POLG mice has been described by recent studies (31, 32). However, the possibility that chronic mild mitochondrial stress also contributes to the pathologic side of the POLG phenotype must also not be discounted. One of the most significant challenges for future studies aimed at therapeutically targeting the mitochondria to increase fat metabolism via FGF21 will be uncoupling the known pathologies intrinsic to mitochondrial damage, disease, and dysfunction from the apparent improvements in metabolic homeostasis. Nevertheless, we believe that the metabolically favorable interaction between FGF21 and dietary fat has the potential to provide new therapeutic avenues to treat the symptoms of both obesity and mitochondrial diseases.

Experimental Procedures

Animals. Male POLG mice (2.5 mo-old) and age-matched wild-type controls (>99% C57BL/6 genetic background) received either a standard chow diet (MI

laboratory rodent diet 5001, Harlan Teklad, 3 kcal/g) or high-fat (60%) diet (F3282, Bio-Serv, 5.5 kcal/g) and water ad libitum up until use for terminal studies at 4.5 mo of age. Mice were housed at 22 °C on a 12-h light/dark cycle. All experimental procedures have been approved by and informed consent was obtained from the Institutional Animal Care and Use Committee at the Salk Institute for Biological Studies.

Gene Expression. Total RNA was isolated from mouse tissue and cells with the TRIzol reagent, and cDNA was subsequently synthesized from 1 μg of RNA using iScript (Bio-Rad). mRNA levels were quantified by qPCR with SYBR Green (Bio-Rad). These experiments were performed in technical triplicates, and relative expression levels were normalized against HPRT mRNA levels in the same RNAs. qPCR primer sequences are available in Table S1.

Metabolomics. Heparinized plasma was collected via submandibular bleed after a 12-h fast under light isoflurane anesthesia and stored at −80 °C until analyzed. LC-MS/MS analysis was performed on extracted metabolites and internal standards as was described (33). The chromatographic peaks were identified by using MultiQuant (v3.0, AB SCIEX), confirmed by manual inspection, and the peak areas was integrated. The median of the peak area of stable isotope internal standards was calculated and used for the normalization of metabolites concentration across the samples and batches. Before multivariate and univariate statistical analysis, the data were log-transformed (13).

Metabolic Studies. Mice were housed in the Oxymax/CLAMS metabolic cage system from Columbus Instruments for 4 d with ad libitum access to food and water. VO2, RER, and activity were measured by the Oxymax system. Body fat composition was determined via MRI. Thermal imaging was performed by using a FLIR T460 infrared camera on unrestrained, alert mice following hair removal from the scapular area, and temperature was quantified by using the FLIR analysis software.

Serum Analyses. Blood was collected during necropsy after a 12-h fast by cardiac puncture. Blood glucose was measured by using the NovaMAX glucometer system. Serum insulin levels (Crystal Chem), leptin (Millipore), FGF21 (Millipore), Ghrelin (Bio-Rad), Resistin (Bio-Rad), and PAI-1 (Bio-Rad) were measured by ELISAs.

Western Blots. Tissue lysates (~100 mg) prepared in RIPA buffer (10 mM Tris·HCl, pH 8.0, 1 mM EDTA, 0.5 mM EGTA, 140 mM NaCl, 1% Triton X-100, 0.1% sodium deoxycholate, 0.1% SDS, and protease/phosphatase inhibitor mixtures) (Roche) were resolved by SDS/PAGE and probed by using primary antibodies specific to Actin (Cell Signaling no. 4970), and UCP1, Mitoprofile, and Porin (Abcam ab10983, ab110413, ab15895).

RNA-Seq. Poly-A mRNA was purified from total RNA isolated from the livers and white fat pads of 4.5-mo-old wild-type and POLG mice fed the aforementioned diets, with three animals in each group. Libraries were prepared by using the Illumina TRUSeq kit as per the manufacturer's instructions. Sequences were referenced against the mouse mm9 reference genome and Gene Ontology was conducted by using the HOMER software suite (homer.salk.edu/homer/).

Histology. Tissues were fixed in 10% (vol/vol) paraformaldehyde, embedded in paraffin, sectioned at 10 μm, and stained with hematoxylin/eosin (Pacific Pathology) or against UCP1 (abcam ab10983). Quantification of histological sections was performed by using the ImageJ software suite. Electron microscopy was performed on BAT from mice perfused with Ringer's solution followed by 0.15 M cacodylate buffer containing 2.5% glutaraldehyde, 2% PFA, and 2 mM $CaCl_2$ at 40 °C for 5 min. Tissues perfused for EM were sectioned, stained, and imaged by the Salk Institute Biophotonics Core.

Adenoviral Preparation. Adenoviral vectors for shFGF21 and shScram were prepared, amplified, and titrated by Vector Biolabs. The targeting sequence used was GGGATTCAACACAGGAGAAC, with a CGAA hairpin loop and TTTTT U6 termination sequence, tagged with eGFP. Adenoviruses were introduced and shRNAs expressed in the liver of young POLG mice via retro-orbital injection.

Statistics. All data are presented as means ± SE. The two-tailed unpaired Student's *t* test or one-way ANOVA with Bonferroni's multiple comparison was used to determine the significance of difference between datasets. These differences were considered statistically significant when $P \leq 0.05$.

ACKNOWLEDGMENTS. We thank J. Alvarez, S. Kaufman, Y. Dai, S. Jacinto, L. Chong, and B. Henriquez for technical assistance, and L. Ong and C. Brondos for administrative assistance. R.M.E. is an Investigator of the Howard Hughes Medical Institute at the Salk Institute and March of Dimes Chair in Molecular and Developmental Biology and is supported by National Institutes of Health Grants DK057978, DK090962, HL088093, and HL105278; The Glenn Foundation for Medical Research; the Leona M. and Harry B. Helmsley Charitable Trust 2012-PG-MED-002; Ipsen/Biomeasure; The Ellison Medical Foundation; and the Samuel Waxman Cancer Research Foundation. R.K.N. is supported by grants from the Jane Botsford Johnson Foundation, the University of California, San Diego (UCSD) Christini Foundation, the UCSD Mitochondrial Research Fund, and the Wright Family Foundation.

1. Yun J, Finkel T (2014) Mitohormesis. *Cell Metab* 19(5):757–766.
2. López-Otín C, Blasco MA, Partridge L, Serrano M, Kroemer G (2013) The hallmarks of aging. *Cell* 153(6):1194–1217.
3. Durieux J, Wolff S, Dillin A (2011) The cell-non-autonomous nature of electron transport chain-mediated longevity. *Cell* 144(1):79–91.
4. Onken B, Driscoll M (2010) Metformin induces a dietary restriction-like state and the oxidative stress response to extend C. elegans Healthspan via AMPK, LKB1, and SKN-1. *PLoS ONE* 5(1):e8758.
5. Rattan SI (2008) Hormesis in aging. *Ageing Res Rev* 7(1):63–78.
6. Trifunovic A, et al. (2004) Premature ageing in mice expressing defective mitochondrial DNA polymerase. *Nature* 429(6990):417–423.
7. Williams SL, et al. (2010) The mtDNA mutation spectrum of the progeroid Polg mutator mouse includes abundant control region multimers. *Cell Metab* 12(6):675–682.
8. Safdar A, et al. (2011) Endurance exercise rescues progeroid aging and induces systemic mitochondrial rejuvenation in mtDNA mutator mice. *Proc Natl Acad Sci USA* 108(10):4135-4140.
9. Kolesar JE, et al. (2014) Defects in mitochondrial DNA replication and oxidative damage in muscle of mtDNA mutator mice. *Free Radic Biol Med* 75:241–251.
10. Trifunovic A, et al. (2005) Somatic mtDNA mutations cause aging phenotypes without affecting reactive oxygen species production. *Proc Natl Acad Sci USA* 102(50):17993–17998.
11. Ahlqvist KJ, et al. (2012) Somatic progenitor cell vulnerability to mitochondrial DNA mutagenesis underlies progeroid phenotypes in Polg mutator mice. *Cell Metab* 15(1):100–109.
12. Zhang Y, et al. (2012) The starvation hormone, fibroblast growth factor-21, extends lifespan in mice. *eLife* 1:e00065.
13. Xia J, Mandal R, Sinelnikov IV, Broadhurst D, Wishart DS (2012) MetaboAnalyst 2.0–a comprehensive server for metabolomic data analysis. *Nucleic Acids Res* 40(Web Server issue):W127–W133.
14. Lowell BB, Flier JS (1997) Brown adipose tissue, beta 3-adrenergic receptors, and obesity. *Annu Rev Med* 48:307–316.
15. Owen BM, et al. (2014) FGF21 acts centrally to induce sympathetic nerve activity, energy expenditure, and weight loss. *Cell Metab* 20(4):670–677.
16. Chartoumpekis DV, et al. (2011) Brown adipose tissue responds to cold and adrenergic stimulation by induction of FGF21. *Mol Med* 17(7-8):736–740.
17. Lee SD, Tontonoz P (2014) Eosinophils in fat: Pink is the new brown. *Cell* 157(6):1249–1250.
18. Petruzzelli M, et al. (2014) A switch from white to brown fat increases energy expenditure in cancer-associated cachexia. *Cell Metab* 20(3):433–447.
19. Wallace DC, Fan W (2009) The pathophysiology of mitochondrial disease as modeled in the mouse. *Genes Dev* 23(15):1714–1736.
20. Inagaki T, et al. (2007) Endocrine regulation of the fasting response by PPARalpha-mediated induction of fibroblast growth factor 21. *Cell Metab* 5(6):415–425.
21. Hondares E, et al. (2010) Hepatic FGF21 expression is induced at birth via PPARalpha in response to milk intake and contributes to thermogenic activation of neonatal brown fat. *Cell Metab* 11(3):206–212.
22. Khan NA, et al. (2014) Effective treatment of mitochondrial myopathy by nicotinamide riboside, a vitamin B3. *EMBO Mol Med* 6(6):721–731.
23. Suomalainen A, et al. (2011) FGF-21 as a biomarker for muscle-manifesting mitochondrial respiratory chain deficiencies: A diagnostic study. *Lancet Neurol* 10(9):806–818.
24. Haas RH, et al.; Mitochondrial Medicine Society's Committee on Diagnosis (2008) The in-depth evaluation of suspected mitochondrial disease. *Mol Genet Metab* 94(1):16–37.
25. Woo YC, Xu A, Wang Y, Lam KS (2013) Fibroblast growth factor 21 as an emerging metabolic regulator: Clinical perspectives. *Clin Endocrinol (Oxf)* 78(4):489–496.
26. Kharitonenkov A, Adams AC (2014) Inventing new medicines: The FGF21 story. *Mol Metab* 3(3):221–229.
27. Wei W, et al. (2012) Fibroblast growth factor 21 promotes bone loss by potentiating the effects of peroxisome proliferator-activated receptor γ. *Proc Natl Acad Sci USA* 109(8):3143–3148.
28. Nygaard EB, Vienberg SG, Ørskov C, Hansen HS, Andersen B (2012) Metformin stimulates FGF21 expression in primary hepatocytes. *Exp Diabetes Res* 2012:465282.
29. Kim KH, et al. (2013) Metformin-induced inhibition of the mitochondrial respiratory chain increases FGF21 expression via ATF4 activation. *Biochem Biophys Res Commun* 440(1):76–81.
30. Scheibye-Knudsen M, et al. (2014) A high-fat diet and NAD(+) activate Sirt1 to rescue premature aging in cockayne syndrome. *Cell Metab* 20(5):840–855.
31. Saleem A, et al. (2015) Polymerase gamma mutator mice rely on increased glycolytic flux for energy production. *Mitochondrion* 21:19–26.
32. Dai Y, et al. (2013) Behavioral and metabolic characterization of heterozygous and homozygous POLG mutator mice. *Mitochondrion* 13(4):282–291.
33. Naviaux JC, et al. (2014) Reversal of autism-like behaviors and metabolism in adult mice with single-dose antipurinergic therapy. *Transl Psychiatr* 4:e400.